3D WAVELET-BASED REGULARIZATION FOR PARALLEL MRI RECONSTRUCTION: IMPACT ON SUBJECT AND GROUP-LEVEL STATISTICAL SENSITIVITY IN FMRI

Lotfi Chaari[1,2], *Sébastien Mériaux*[2], *Solveig Badillo*[2], *Philippe Ciuciu*[2] *and Jean-Christophe Pesquet*[1]

[1] Université Paris-Est, IGM and UMR-CNRS 8049,
77454 Marne-la-Vallée cedex, France
{chaari,pesquet}@univ-mlv.fr

[2] CEA/DSV/I^{2}BM/Neurospin, CEA Saclay, Bbt. 145,
Point Courrier 156, 91191 Gif-sur-Yvette cedex, France
{sebastien.meriaux,solveig.badillo,philippe.ciuciu}@cea.fr

ABSTRACT

Parallel MRI is a fast imaging technique that allows reconstruction of full Field-of-View (FoV) images based on undersampled k-space data acquired using multiple receiver coils with complementary sensitivity profiles. It enables the acquisition of highly resolved images either in space or in time, which is of particular interest in applications like functional neuroimaging. These improvements are counterbalanced by a degraded SNR and the presence of artifacts that depend on the reconstruction algorithm. To improve the performance of the widely used SENSE algorithm, 2D regularization in the wavelet domain has recently been efficiently investigated [1]. In this paper, we extend this work to 3D-wavelet decompositions in order to manipulate all slices together. We illustrate the gain induced by such extension in terms of statistical impact on functional MRI (fMRI) data analysis using a fast-event related protocol. Our results show that our 3D reconstruction algorithm outperforms its 2D counterpart and the SENSE algorithm in several statistical respects at the group-level: peak localization, local maxima, cluster extent, robustness to high acceleration factors.

1 Introduction

Parallel imaging in Magnetic Resonance Imaging (pMRI) aims at reducing acquisition time in clinical applications or at improving spatial or temporal resolution of acquired images in neuroimaging. Many methods like GRAPPA (Generalized Autocalibrating Partially Parallel Acquisitions) [2] and SENSE (SENSitivity Encoding) [3] have been proposed in the literature to reconstruct a full FoV image from multiple k-space under-sampled images acquired on separate channels. GRAPPA-based reconstruction operates in the k-space, while SENSE proceeds in the image domain (after an inverse Fourier transform of reduced FoV images). Another difference is that GRAPPA is autocalibrated, while SENSE needs a separate coil sensitivity estimation step based on a reference scan. Note however that an autocalibrated version of SENSE is also available for instance in Siemens scanners and called mSENSE hereafter. All these methods may suffer from strong artifacts when high values of acceleration factors R are considered in the imaging setup or when they are applied to Echo Planar Images (EPI), which are acquired during fMRI experiments. These artifacts can drastically disturb subsequent analysis such as brain activation detection in functional neuroimaging. Regularized SENSE methods have been proposed in the literature to improve the robustness of the solution [1, 4–6]. Some of them apply quadratic regularization while others resort to edge-preserving regularization in the wavelet transform domain. To the best of our knowledge only one study has been conducted to assess the impact of using a specific pMRI reconstruction algorithm on brain activation detection in fMRI [7]. There are several underlying reasons for this: first, all pMRI algorithms are not available on a specific scanner. Second, reconstructing the full FoV image with an external pMRI algorithm requires to get and read the huge *raw* data files from the MRI scanner, then reconstruct all reduced FoV images using a *home-made* reconstruction pipeline that embodies ghosting EPI artifact corrections and k-space regridding, before applying the proposed pMRI method to each volume of the fMRI series. In [7], we have only reported statistical results at the subject level while strong between-subject differences may exist in terms of brain activity due to between-subject anatomical and functional variability. To this end, the present work aims at achieving reproducibility and robustness at the group level. In addition, we bring some evidence that 3D wavelet-based regularization is more advantageous for brain activity detection in comparison with 2D transforms due to its ability to capture spatial dependencies through adjacent slices in order to better reduce reconstruction artifacts. Hence, we conduct a statistical comparison between different pMRI reconstruction algorithms (mSENSE, 1D-UWRSENSE proposed in [1, 7] and 3D-UWRSENSE) for detecting brain activity elicited during a cognitive event-related protocol in fMRI. We also show that a significant gain in spatial in-plane resolution ($2 \times 2\text{mm}^2$) can be achieved using $R = 2$ at a constant time of repetition (TR, ie the between-scan time interval) without sacrificing the statistical sensitivity if a wavelet-based regularized algorithm is involved in the pipeline. To this end, the reconstructed full FoV images are analysed in the General Linear Model (GLM) framework using SPM5 [1]. Our particular interest is to demonstrate that when artifacts are superimposed to brain activation, this directly impacts subsequent statistical analysis.

2 Parallel imaging in MRI

In parallel MRI, an array of L coils is employed to measure the spin density $\overline{\rho}$ into the object under investigation.[2] Since

Invited paper in the special session on *Wavelets in neuroimaging*

[1] `http://www.fil.ion.ucl.ac.uk`

[2] The overbar is used to distinguish the "true" data from a generic variable.

most MRI sequences correspond to a 2D acquisition scheme, the signal $\widetilde{d}_\ell$ received by each coil ℓ is the Fourier transform of the desired 2D field $\overline{\rho} \in \mathbb{R}^{Y \times X}$ on the specified FoV weighted by the coil sensitivity profile s_ℓ, evaluated at some location $\boldsymbol{k}_r = (k_y, k_x)^\mathsf{T}$ in the k-space:

$$\widetilde{d}_\ell(\boldsymbol{k}_r) = \int \overline{\rho}(\boldsymbol{r}) s_\ell(\boldsymbol{r}) e^{-\imath 2\pi \boldsymbol{k}_r^\mathsf{T} \boldsymbol{r}} \, d\boldsymbol{r} + \widetilde{n}_\ell(\boldsymbol{k}_r), \qquad (1)$$

where $\widetilde{n}_\ell(\boldsymbol{k}_r)$ is a coil-dependent additive zero-mean circular Gaussian noise, which is independent and identically distributed (iid) in the k-space, and $\boldsymbol{r} = (y, x)^\mathsf{T} \in Y \times X$ is the spatial position in the image domain. For the sake of simplicity, a Cartesian coordinate system is generally adopted in neuroimaging. In parallel MRI, the sampling period along the phase encoding direction is R times larger than the one used for conventional acquisition, $R \leq L$ being the reduction factor. To recover full FoV images, an unfolding step has to be performed. In what follows, we focus on SENSE-like methods operating in the space domain. A 2D inverse Fourier transform allows us first to recover the measured signal in the spatial domain. By accounting for the k-space undersampling at R rate, the inverse Fourier transform gives us the spatial counterpart of Eq. (1) in matrix form:

$$\boldsymbol{d}(\boldsymbol{r}) = \boldsymbol{S}(\boldsymbol{r}) \overline{\boldsymbol{\rho}}(\boldsymbol{r}) + \boldsymbol{n}(\boldsymbol{r}), \qquad (2)$$

where $\overline{\boldsymbol{\rho}}(\boldsymbol{r}) \triangleq [\overline{\rho}(y, x), .., \overline{\rho}(y + (R-1)\Delta y, x)]^\mathsf{T}$,

$$\boldsymbol{S}(\boldsymbol{r}) \triangleq \begin{bmatrix} s_1(y,x) & \dots & s_1(y+(R-1)\Delta y, x) \\ \vdots & \vdots & \vdots \\ s_L(y,x) & \dots & s_L(y+(R-1)\Delta y, x) \end{bmatrix},$$

$\boldsymbol{d}(\boldsymbol{r}) \triangleq [d_1(y,x), .., d_L(y,x)]^\mathsf{T}$, $\boldsymbol{n}(\boldsymbol{r}) \triangleq [n_1(y,x), .., n_L(y,x)]^\mathsf{T}$, $\Delta y = \frac{Y}{R}$ being the aliasing period and y and x the positions in the image domain along the phase and encoding directions, respectively. Based on this model, the reconstruction step consists of solving Eq. (2) and recovering $\overline{\boldsymbol{\rho}}(\boldsymbol{r})$ from $\boldsymbol{d}(\boldsymbol{r})$ and $\boldsymbol{S}(\boldsymbol{r})$ at each spatial positions $\boldsymbol{r} = (y, x)^\mathsf{T}$. The *sensitivity* matrix $\boldsymbol{S}(\boldsymbol{r})$ is estimated using a reference scan and varies according to the coil geometry. Note that the coil images $(d_\ell)_{1 \leq l \leq L}$ as well as the sought image $\overline{\rho}$ are complex-valued, although $|\overline{\rho}|$ is considered for visualization only.

3 Reconstruction algorithms

For the sake of conciseness, all pMRI reconstruction algorithms considered here minimize an objective function of the following form:

$$\mathcal{J}(\rho) = \sum_{\mathbf{r}} \| \boldsymbol{d}(\boldsymbol{r}) - \boldsymbol{S}(\boldsymbol{r}) \boldsymbol{\rho}(\boldsymbol{r}) \|^2_{\boldsymbol{\Psi}^{-1}} + \kappa_1 \Phi(\rho) + \kappa_2 i_{\mathcal{M}}(\rho), \quad (3)$$

where $\kappa_1, \kappa_2 \geq 0$ are two constants, and Φ and $i_{\mathcal{M}}$ are two functions to be specified. The noise covariance matrix $\boldsymbol{\Psi}$ is usually estimated based on L acquired images $(\underline{\mathrm{d}}_\ell)_{1 \leq \ell \leq L}$ from all coils without radio frequency pulses.
Since any MRI volume is usually acquired as a stack of 2D slices, most parallel reconstruction methods take place in 2D and try to invert Eq. (3) for each slice separately. The volume reconstruction thus consists in iterating over slices.

3.1 SENSE imaging

In its simplest form, SENSE imaging amounts to solving a one-dimensional inversion problem due to the separability of the Fourier transform. Note however that this inverse problem admits a two-dimensional extension in 3D imaging sequences like Echo Volume Imaging (EVI) [8] where undersampling occurs in two k-space directions. The SENSE reconstruction [3] actually minimizes a Weighted Least Squares (WLS) criterion $\mathcal{J}_{\mathrm{WLS}}$ which can be derived by setting $\kappa_1 = \kappa_2 = 0$ in Eq. (3). Hence, the SENSE full FoV image is simply the maximum likelihood estimate under Gaussian noise assumptions and reads at the position $\boldsymbol{r}$:

$$\widehat{\boldsymbol{\rho}}_{\mathrm{WLS}}(\boldsymbol{r}) = \left(\boldsymbol{S}^\mathsf{H}(\boldsymbol{r}) \boldsymbol{\Psi}^{-1} \boldsymbol{S}(\boldsymbol{r})\right)^\sharp \boldsymbol{S}^\mathsf{H}(\boldsymbol{r}) \boldsymbol{\Psi}^{-1} \boldsymbol{d}(\boldsymbol{r}), \qquad (4)$$

where $(\cdot)^\mathsf{H}$ (resp. $(\cdot)^\sharp$) stands for the transposed complex conjugate (resp. pseudo-inverse). In practice, the performance of the SENSE method is limited because of the presence of *i)* distortions in the measurements $\boldsymbol{d}(\boldsymbol{r})$, *ii)* the putative ill-conditioning of $\boldsymbol{S}(\boldsymbol{r})$ at locations $\boldsymbol{r}$ close to the image center and *iii)* the presence of errors in the estimation of $\boldsymbol{S}(\boldsymbol{r})$ mainly at brain/air interfaces. To improve the robustness of the solution to this ill-posed problem, regularization is usually used. As investigated in [1, 6], regularization using 2D Wavelet Transforms (WTs) is a powerful tool to improve SENSE reconstruction. In what follows, we extend this strategy by using 3D-decompositions in order to account for cross-slice continuity. Indeed, 3D wavelets enables to smooth reconstruction artifacts along the slice selection direction, which remained inaccessible using 2D reconstruction.

3.2 3D-UWR-SENSE

Let T be the WT operator which corresponds to a discrete decomposition onto a separable 3D dyadic orthonormal wavelet basis performed over $j_{\max}$ resolution levels. The full FoV image $\overline{\rho}$ of size $Y \times X \times Z$ can be seen as an element of the Euclidean space $\mathbb{C}^K$ with $K = Y \times X \times Z$ endowed with the standard inner product $\langle \cdot \mid \cdot \rangle$ and norm $\| \cdot \|$. The resulting wavelet coefficient field of a target image function ρ is defined by $\zeta = \left((\zeta_{a,k})_{1 \leq k \leq K_{j_{\max}}}, (\zeta_{o,j,k})_{1 \leq j \leq j_{\max}, 1 \leq k \leq K_j}\right)$ where $K_j = K 2^{-2j}$ is the number of wavelet coefficients in a given subband at resolution j (by assuming that Y, X and Z are multiple of $2^{j_{\max}}$) and the coefficients have been reindexed in such a way that $\zeta_{a,k}$ denotes an approximation coefficient at resolution level $j_{\max}$ and $\zeta_{o,j,k}$ denotes a detail coefficient at resolution level j and orientation $o \in \{h, v, d\}$ (h, v and d stand for *horizontal*, *vertical* and *diagonal*, respectively).
From a Bayesian viewpoint, regularization consists of injecting some a priori knowledge about the optimal solution. The computation of the minimizer of $\mathcal{J}$ therefore consists of finding the Maximum a Posteriori (MAP) solution based on the likelihood and the prior distribution. In our case, this prior involves $\overline{\zeta} = T\overline{\rho}$, the forward WT of the sought image $\overline{\rho}$. Here, we assume that the probability density function (pdf) of the corresponding real and imaginary parts of the wavelet coefficients ζ is a generalized Gaussian distribution (GG). Hence, for each coefficient ξ in a given sub-band $\zeta_{o,j,k}$ ($o \in \{a, h, v, d\}$), the neg-log prior pdf (up to an additive constant) is given by

$$\begin{aligned} \Phi_{o,j}(\xi) =& \Phi^{\mathrm{Re}}_{o,j}(\xi) + \Phi^{\mathrm{Im}}_{o,j}(\xi) \\ =& (\omega^{\mathrm{Re}}_{o,j} |\mathrm{Re}(\xi)|)^{\beta^{\mathrm{Re}}_{o,j}} + (\omega^{\mathrm{Im}}_{o,j} |\mathrm{Im}(\xi)|)^{\beta^{\mathrm{Im}}_{o,j}}. \end{aligned} \qquad (5)$$

Hereabove, Re(·) and Im(·) (or $\cdot^{\mathrm{Re}}$ and $\cdot^{\mathrm{Im}}$) stand for the real and imaginary parts, respectively. Note that $(\omega_{o,j}^{\mathrm{Re}}, \omega_{o,j}^{\mathrm{Im}}) \in \mathbb{R}_+^2$, $\beta_{o,j}^{\mathrm{Re}} \geq 1$ and $\beta_{o,j}^{\mathrm{Im}} \geq 1$ are hyper-parameters, which have to be estimated. In [1], we automatically tuned these statistical parameters in the maximum likelihood sense on the SENSE-based reconstructed image. In order to achieve more robust reconstruction and avoid noise outside the brain mask for instance, another penalty may be considered in the regularization term. This additional prior is simply an indicator function $i_{\mathcal{M}}$ on the brain mask $\mathcal{M}$ [3]. When $\kappa_1 = \kappa_2 = 1$, the criterion in Eq. (3) writes:

$$\mathcal{J}_{\mathrm{WT}}(\rho) = \sum_{\boldsymbol{r}} \| \boldsymbol{d}(\boldsymbol{r}) - \boldsymbol{S}(\boldsymbol{r})\boldsymbol{\rho}(\boldsymbol{r}) \|_{\boldsymbol{\Psi}^{-1}}^2 + \Phi(T\rho) + i_{\mathcal{M}}(\rho), \quad (6)$$

where $\Phi(T\rho) = \sum_k \Phi_a((T\rho)_{a,k}) + \sum_o \sum_j \sum_k \Phi_{o,j}((T\rho)_{o,j,k})$ and $\boldsymbol{r} = (y, x, z)$ is the 3D spatial position, $z \in \{1, \ldots, Z\}$ being the position along the third direction (slice selection). Although this criterion is convex, it cannot be optimized using standard algorithms like pseudo-conjugate gradient since it is not differentiable. To address this problem, many recent algorithms have been proposed in the convex optimization literature dealing with non-differentiable criteria like FISTA [9] or Forward-Backward [10]. However, most of them are designed for solving convex criteria including only the sum of two functions, whereas our criterion is the sum of three convex functions. For this reason, we will use the PPXA algorithm [11] which enables the optimization of $m \in \mathbb{N}$ functions, provided that, for each of them the proximity operator admits a closed form expression [11]. To summarize, our methodological contribution also called 3D-UWR-SENSE algorithm minimizes the regularized criterion in Eq. (6) using the PPXA algorithm. The PPXA parameters have been adjusted to ensure faster convergence [11].

4 Experimental results

4.1 Data acquisition

The fMRI data were recorded at 3 Tesla on a Siemens Trio magnet using a Gradient-Echo EPI (GE-EPI) sequence ($TE = 30$ ms, $TR = 2,4$ s, slice thickness = 3 mm, transversal orientation, FoV = 192 mm^2) during a cognitive localizer experiment designed to map auditory, visual and motor brain functions as well as higher cognitive tasks such as number processing and language comprehension. It consisted of a single session of $N = 128$ scans. The paradigm was a fast event-related design comprising sixty auditory, visual and motor stimuli, defined in ten experimental conditions (auditory and visual sentences, auditory and visual calculations, left/right auditory and visual clicks, horizontal and vertical checkerboards). A $L = 32$ channels coil was used to enable parallel imaging. Fifteen subjects gave informed consent to be scanned. In each subject, fMRI data were collected at different in-plane spatial resolutions (3×3 and 2×2 mm^2). The mSENSE algorithm available on the Siemens workstation was used with varying the acceleration factor ($R = 2$ or $R = 4$).

4.2 Reconstruction comparison

Acquired data were first reconstructed using the black-box Siemens pipeline available on the Workstation. Since we also recorded the *raw* or un-reconstructed data, we enabled the comparison with our own reconstruction pipeline, which proceeds as follows for EPI images: *i) k-space regridding and de-oversampling*: to account for non-uniform k space sampling, which occurs in fast MRI sequences like GE-EPI; *ii) EPI correction* to remove the EPI Nyquist ghost artifacts due to the odd-even echo inconsistencies; *iii) Estimation of the sensitivity maps*. These maps were obtained as proposed in [3] by dividing the coil-specific images by the module of the Sum Of Squares images, which are calculated based on an acquisition of the k-space center (24 lines) before the N scans; *iv)* L single channel reduced FoV reconstructions by inverse Fourier transform on corrected EPI images; *v)* 3D-UWR-SENSE reconstruction for each scan separately (parallel processing). In an eight-CPU computer (Intel Xeon `W3520@2.67GHz`), the complete procedure takes about 2 h 30 min, by loading the reconstruction of 16 scans per CPU. For comparison purpose, Fig. 1 shows typical examples of reconstructed images using the mSENSE and 3D-UWR-SENSE algorithms for $R = 2$ and $R = 4$ with 2×2mm^2 in-plane resolution. These figures

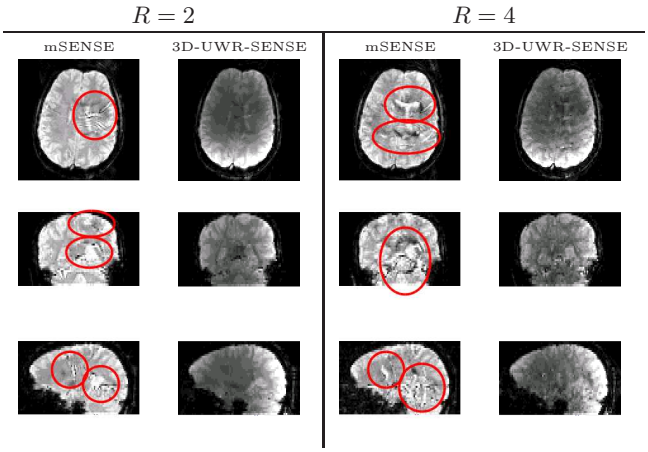

Fig. 1. **Axial** (top), **coronal** (middle) and **sagittal** (bottom) reconstructed slices using mSENSE, and 3D-UWR-SENSE for $R = 2$ and $R = 4$ with 2×2 mm^2 in-plane spatial resolution. Red circles indicate reconstruction artifacts.

easily show that our pipeline allows to achieve more accurate reconstruction than the mSENSE algorithm in terms of reconstruction artifacts. In fact, the mSENSE reconstructed images present artifacts located at the center and image borders, which may be nasty in activation detection in these area such as temporal lobes. Note that these conclusions are reproducible across subjects although the artifacts may appear on different slices (see red circles). Note also that, in contrast to the Siemens reconstruction, our pipeline do not involve any signal homogeneity filter that may introduce some bias in the voxel intensities. Through illustrated images, it is clear that 3D-UWR-SENSE provides better full FoV images than mSENSE. In Fig. 1 ($R = 2$), it is shown that mSENSE generates strong artifacts in the right temporal lobe (on the left side) and in the left frontal lobe (on the right side) of the slice, while our 3D-UWR-SENSE still gives quite accurate reconstruction. For $R = 4$, it is also clear that the mSENSE algorithm induces strong artifacts close to the deep cerebellar nuclei, which are completely removed using our algorithm. Note that these conclusions are reproducible across subjects.

[3] $\forall \rho \in \mathbb{C}^K, i_{\mathcal{M}}(\rho) = \sum_{\boldsymbol{r}} i_0(\rho(\boldsymbol{r}))$ where $i_0(\rho(\boldsymbol{r})) = 0$ if $\boldsymbol{r} \in \mathcal{M}$ and $+\infty$ otherwise

4.3 Impact on brain activity detection

Also, we quantitatively compare the performance of mSENSE and 3D-UWR-SENSE pMRI reconstruction algorithms for brain activity detection at the subject- and group-level on $2 \times 2 \times 3\text{mm}^3$ EPI data. fMRI data analysis has been conducted using SPM5 in which the design matrix shown in Fig.2 relying on ten regressors has been built up. Standard neuroimaging preprocessing was applied using the SPM5 software: after motion correction, cerebral volumes were realigned to an inter-subject template and smoothed with a 5 mm isotropic Gaussian kernel. Next, brain activity detection at the subject-level was performed by defining the design matrix shown in Fig. 2, estimating the effect sizes and computing the statistical T-maps associated with the contrasts of interest. Finally, group-level validation was carried out.

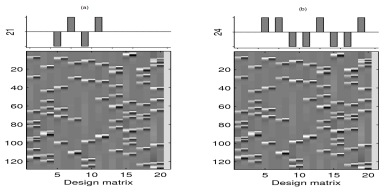

Fig. 2. (a): design matrix and the `Lc-Rc` contrast involving two conditions (auditory and visual modalities); (b): design matrix and the `A-V` contrast involving four conditions (sentence, computation, left click, right click). The design matrix is made up of twenty regressors corresponding to the canonical HRF and its time derivative for each of the ten experimental conditions, in addition to a mean signal regressor.

Here, we only report results involving the Left click vs. Right click (`Lc-Rc`) and Auditory vs. Visual (`A-V`) contrasts since the expected activations, which lie in different parts of the brain, can be putatively corrupted by reconstruction artifacts. The results are reported in terms of Student-t statistical maps thresholded at a $p = 0.05$ p-value corrected for multiple comparisons [12] as well as statistical tables that provide cluster- and voxel-level p-values, maximal T-scores and corresponding locations of these peaks.

4.3.1 Subject-level results

In Fig. 3, it is shown that the 3D-UWR-SENSE approach enables the recovery of expected bilateral activations in the temporal lobes elicited by speech perception and comprehension involved in the `A-V` contrast, while the mSENSE method retrieved smaller clusters: activation cluster in the left hemisphere is somehow lost due to strong reconstruction artifacts. This result holds both for $R = 4$ and $R = 2$ (results not shown for $R = 2$). The `A-V` contrast defines a compound comparison which involves the same stimuli presented either in the visual or auditory modality, respectively. In this sense, this comparison aims only at localizing sensory brain areas, i.e. the primary auditory cortices. For the `Lc-Rc` contrast, Fig. 4 shows that the 3D-UWR-SENSE algorithm allows the detection of expected activated areas in the contralateral motor cortex missed by the mSENSE algorithm for $R = 4$. This result holds also for $R = 2$ (results not shown). The `Lc-Rc` contrast defines a compound comparison which involves two stimuli which are also presented either in the visual or auditory modality. This comparison aims therefore at detecting lateralization effect in the motor cortex.

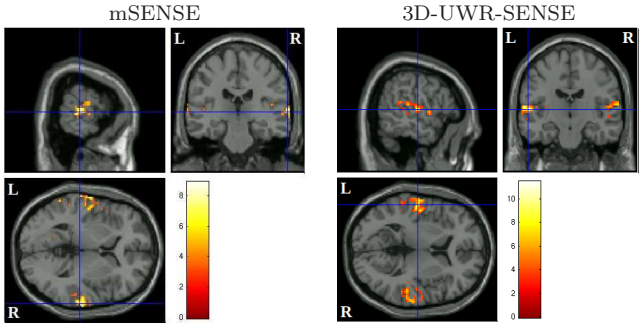

Fig. 3. Student-t maps superimposed to anatomical MRI for the `A-V` contrast and $R = 4$.

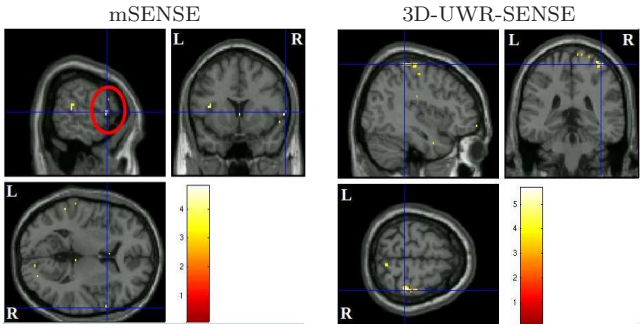

Fig. 4. Student-t maps superimposed to anatomical MRI for the `Lc-Rc` contrast and $R = 4$.

4.3.2 Group-level results

In this fMRI study, random effect analysis has been used for group-level validation involving fifteen healthy subjects of the acquired database. For the `A-V` and `Lc-Rc` contrasts, Maximum Intensity Projection (MIP) student-t maps for $R = 4$ are provided in Figs. 5-6. Fig. 5 clearly shows that for the `A-V` contrast, our pipeline allows to better detect expected significant bitaleral activations than the Siemens pipeline. For comparison purpose, our pipeline involves here the 3D-UWR-SENSE method, as well as the 1D-UWR-SENSE one which has been validated on the suject-level in [7]. From a quantitative viewpoint, results for the most significant clusters are provided for the `A-V` contrast in Table 1. Voxel and cluster-level results show that our pipeline outperforms the mSENSE reconstruction in terms of clusters size and T-score maxima. For the `Lc-Rc` contrast, Fig. 6 shows that our pipeline allows to detect much more spatially extended activation areas in the motor cortex. Quantitatively speaking, Table 2 shows that the detected clusters using our pipeline reconstruction are of larger size and higher T-score maxima than the ones detected based on the mSENSE reconstruction. These results are valid both for $R = 4$ and $R = 2$ (results not shown for $R = 2$). It is also worth noticing that detected activated area using our pipeline reconstruction are more excentric that with the mSENSE reconstruction, which has actually been expected regarding to the motor cortex location.

5 Conclusion

In this contribution, we examined the impact of the pMRI reconstruction algorithm on the statistical performance for brain activity detection in BOLD fMRI data. At the subject- and group-level (3 T), we showed that our 3D-UWR-SENSE

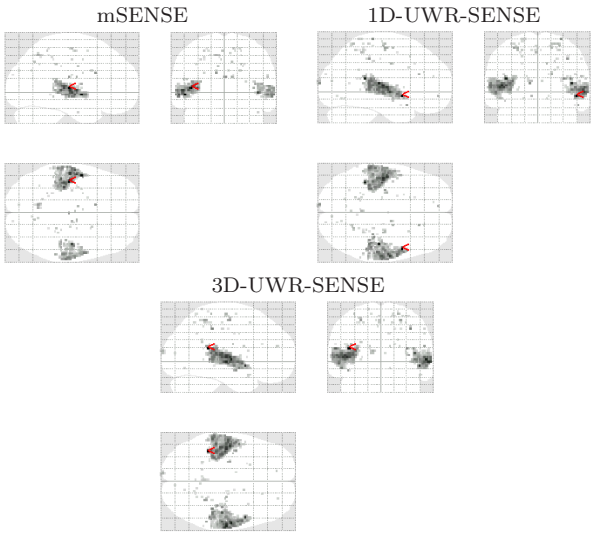

Fig. 5. Group-level student-t maps for the `A-V` contrast. Data have been reconstructed using the mSENSE, 1D-UWR-SENSE and 3D-UWR-SENSE for $R = 4$. Neurological convention: left is left. Red arrows indicate the global maxima.

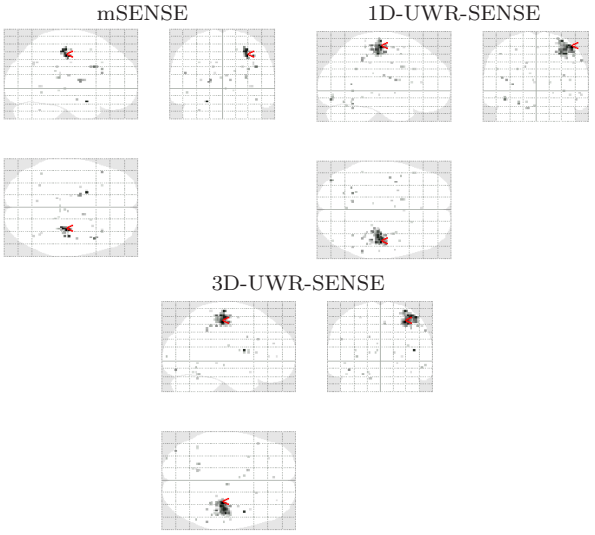

Fig. 6. Group-level student-t maps for the `Lc-Rc` contrast. Data have been reconstructed using the mSENSE, 1D-UWR-SENSE and 3D-UWR-SENSE for $R = 4$. Neurological convention: left is left. Red arrows indicate the global maxima.

Table 1. Significant statistical results at the group-level for the `A-V` contrast (corrected for multiple comparisons at $p = 0.05$). Images were reconstructed using the mSENSE, 1D-UWR-SENSE and 3D-UWR-SENSE algorithm for $R = 4$.

	cluster-level		voxel-level		
	p-value	Size	p-value	T-score	Position
mSENSE	$< 10^{-3}$	424	0.002	9.86	-42 -18 6
	$< 10^{-3}$	222	0.048	7.76	44 -14 0
1D-UWR-SENSE	$< 10^{-3}$	639	0.008	10.64	-40 -40 18
	$< 10^{-3}$	555	0.002	9.52	50 8 -6
3D-UWR-SENSE	$< 10^{-3}$	**784**	0.001	**11.06**	-40 -40 18
	$< 10^{-3}$	658	0.012	9.93	58 -10 3

algorithm outperforms the mSENSE one both qualitatively and quantitatively from a statistical viewpoint. We showed how the choice of the pMRI reconstruction algorithm enables whole brain neuroscience studies at high spatial resolution, even when comparing subtle contrasts. Future work will concern the statistical comparison at higher in-plane resolution (1.5×1.5 mm^2), which is only rechable using $R = 4$.

Table 2. Significant statistical results at the group-level for the `Lc-Rc` contrast (corrected for multiple comparisons). Images were reconstructed using the mSENSE, 1D-UWR-SENSE and 3D-UWR-SENSE algorithm for $R = 4$.

	cluster-level		voxel-level		
	p-value	Size	p-value	T-score	Position
mSENSE	$< 10^{-3}$	38	0.990	5.97	32 -20 45
1D-UWR-SENSE	$< 10^{-3}$	163	0.128	**7.51**	46 -18 60
3D-UWR-SENSE	$< 10^{-3}$	**174**	0.182	7.27	32 -22 54

6 References

[1] L. Chaari, J.-C. Pesquet, A. Benazza-Benyahia, and Ph. Ciuciu, "A wavelet-based regularized reconstruction algorithm for SENSE parallel MRI with applications to neuroimaging," *Medical Image Analysis*, 2011, doi:10.1016/j.media.2010.08.001, In press.

[2] M. A. Griswold, P. M. Jakob, R. M. Heidemann, M. Nittka, V. Jellus, J. Wang, B. Kiefer, and A. Haase, "Generalized autocalibrating partially parallel acquisitions GRAPPA," *Mag. Res. in Med.*, vol. 47, no. 6, pp. 1202–1210, Jun. 2002.

[3] K. P. Pruessmann, M. Weiger, M. B. Scheidegger, and P. Boesiger, "SENSE: sensitivity encoding for fast MRI," *Mag. Res. in Med.*, vol. 42, no. 5, pp. 952–962, Jul. 1999.

[4] Z. P. Liang, R. Bammer, J. Ji, N. J. Pelc, and G. H. Glover, "Making better SENSE: wavelet denoising, Tikhonov regularization, and total least squares," in *Int. Soc. for Mag. Res. in Med.*, Hawaï, USA, May 18-24 2002, p. 2388.

[5] Y. M. Zou, L. Ying, and B. Liu, "SparseSENSE: application of compressed sensing in parallel MRI," in *IEEE International Conference on Technology and Applications in Biomedicine*, Shenzhen, China, May 30-31 2008, pp. 127–130.

[6] B. Liu, E. Abdelsalam, J. Sheng, and L. Ying, "Improved spiral SENSE reconstruction using a multiscale wavelet model," in *IEEE International Symp. on Biomed. Imag.*, Paris, France, May 14-17 2008, pp. 1505–1508.

[7] L. Chaari, S. Mériaux, J.-Ch. Pesquet, and Ph. Ciuciu, "Impact of the parallel imaging reconstruction algorithm on brain activity detection in fMRI," in *Proc. IEEE Int. Symp. on App. Sci. in Biomed. and Comm. Tech. (ISABEL)*, Rome, Italy, Nov. 7-10 2010, 4p.

[8] C. Rabrait, Ph. Ciuciu, A. Ribès, C. Poupon, P. Leroux, V. Lebon, G. Dehaene-Lambertz, D. Le Bihan, and F. Lethimonnier, "High temporal resolution functional MRI using parallel echo volume imaging," *Mag. Res. in Med.*, vol. 27, no. 4, pp. 744–753, Mar. 2008.

[9] A. Beck and M. Teboulle, "A Fast Iterative Shrinkage-Thresholding Algorithm for Linear Inverse Problems," *SIAM Journal on Imaging Sciences*, vol. 2, no. 1, pp. 183–202, 2009.

[10] C. Chaux, P. Combettes, J.-C. Pesquet, and V.R Wajs, "A variational formulation for frame-based inverse problems," *Inv. Problems*, vol. 23, no. 4, pp. 1495–1518, Aug. 2007.

[11] P. L. Combettes and J.-C. Pesquet, "A proximal decomposition method for solving convex variational inverse problems," *Inv. Problems*, vol. 24, no. 6, 2009.

[12] J. Ashburner, K. J. Friston, and W. Penny, *Human Brain Function, J. Ashburner, K. Friston and W. Penny Eds*, chapter Introduction to Random Field Theory, Academic Press, 2nd edition, 2004.